Wavelet Neural Network-Based Controller Design for Magnetic Levitation System

Abdulla Ibrahim Abdulla [1], Mohammed Qasim [2*], Mohammed Almaged [3]
[1, 2, 3] Department of Systems and Control Engineering, Ninevah University, Mosul, Iraq
Email: [1] abdullah.abdullah@uoninevah.edu.iq, [2] mohammed.qasim@uoninevah.edu.iq,
[3] mohammed.younus@uoninevah.edu.iq
*Corresponding Author

Abstract*—The magnetic levitation system (MLS) poses a substantial control challenge owing to its intrinsic instability and pronounced nonlinear dynamics. The implementation of robust control methodologies is imperative to guarantee stable operational performance, particularly in environments characterized by external disturbances and parametric uncertainties. This study investigates the development of a PID-like control strategy for a magnetic levitation system (MLS), employing WNN architecture. The parameters of the proposed controller are optimized by employing Fick's Law Algorithm (FLA). The optimization process utilizes a cost function that comprises a weighted sum of the Integral Time-weighted Square Error (ITSE), Integral Time-weighted Absolute Error (ITAE), maximum overshoot (MO), and minimum undershoot (MU). This multi-objective cost function enables a comprehensive evaluation of the controller's performance across various criteria. A square wave reference signal is employed to conduct the optimization process, presenting a challenging test case for control system performance due to its abrupt transitions. The efficacy of the proposed controller is evaluated through a comparative analysis with a conventional PID controller. Comparative simulations are conducted employing three distinct reference trajectories: step, sinusoidal, and square waves. These diverse trajectories provide a comprehensive evaluation of the controller's performance. To assess the robustness of the proposed controller, simulations are conducted within the MATLAB/Simulink environment, subjecting the MLS model to both external disturbances and parametric uncertainties. The developed controller exhibits superior performance and robustness characteristics in comparison to the conventional PID controller. It effectively attenuates the detrimental impact of both parametric uncertainties and external disturbances, while concurrently maintaining a high degree of performance accuracy in terms of overshoot, steady-state error, and energy consumption.

Keywords—Wavelet Neural Network; Magnetic Levitation System; Fick's Law Algorithm; External Disturbances; Parameter Uncertainties.

I. INTRODUCTION

Magnetic Levitation System is a single input, a single output (SISO) nonlinear system that is extremely unstable [1]-[6]. The fundamental idea behind a magnetic levitation device is to use current-generated electromagnetic forces to counteract the force of gravity on the levitated object [7][8]. The nonlinear differential equation of the third order represents the MLS mathematical model constructed from the state variables: the vertical position of the levitated object, the coil current, and the object's velocity [9]. MLS control's primary goal is to provide robust tracking and anti-interference capabilities to the system. The benefits of MLS include reduced energy use, no friction, and more. Numerous applications in engineering and education have made use of it, including magnetic levitation wind turbines [10][11], magnetic levitation trains [12]-[14], magnetic levitation in medicine [15], and magnetic levitation bearings [16]-[18]. For engineering applications, controller design is crucial, and MLS control is a significant and alluring area of control study [19][20].

Many control algorithms exist in the literature such as PID controller [21][22], fractional-order PID controller [23], sliding mode controller [24], model predictive controller [25]-[29], passivity-based adaptive controller [30][31], vision-based controller [32][33]. The adaptive fuzzy controller was implemented in [34]-[36]. Nonetheless, adjusting the fuzzy controls' parameters, such as the number of rules and the kind of membership functions is challenging. The robust H-infinity controller has been applied for MLS controlling [37]-[39]. However, the intricacy of the design necessitates sophisticated mathematics and meticulous adjustment of weighting factors. The sliding mode controller has been used to control MLS [40][41]. However, the chattering effect brought on by discontinuous control is the main disadvantage of the SMC. The backstepping controller is proposed in [42][43] for controlling the MLS. Whereas, each stage of the backstepping control procedure depends on the designer's ability to provide a valid Lyapunov function that can be used to build a control rule. In [44]-[46] the feedback linearization-based controller is used to control the MLS. Nevertheless, any disturbances that affect the MLS can largely affect how it reacts when utilizing the feedback linearization control.

Recently, Artificial Neural Network (ANN)-based intelligent controllers were proposed to avoid the abovementioned problems of the MLS [47]-[49]. Accordingly, because of their adaptive capabilities and robust self-learning, ANNs can enhance the performance of MLS trajectory tracking [50]. For instance, a radial basis function neural network (RBFNN)-based model predictive controller has outpaced the traditional PID controller in terms of trajectory tracking performance of MLS [51][52]. An adaptive sliding mode controller (SMC) based on an RBFNN surpassed the conventional SMC approach regarding resilience and convergence speed of MLS trajectory tracking [53][54]. To reduce the MLS's trajectory tracking error, a

backpropagation neural network (BPNN)-based feedback compensation and fuzzy controllers were suggested [55][56].

The wavelet neural network-based controllers perform better than the aforementioned neural networks on trajectory-tracking tasks which require precise, robust, and instantaneous control of MLS [57][58]. The controller based on WNN is superior due to its robustness to noise, faster learning, improved nonlinear approximation, and localized time-frequency representation. These advantages result in superior performance, increased dependability, and reduced processing needs compared to traditional neural networks.

This study presents a PID-like controller using a modified ridge wavelet neural network for trajectory tracking of MLS while ensuring a particular control performance against model uncertainties and external disturbances. The straightforwardness and dependability of PID control, together with the flexibility and nonlinear approximation abilities of WNN are merged for MLS trajectory tracking. Improved performance, robustness, and efficacy are the outcomes of this synergy, which makes it especially useful for systems requiring great accuracy and flexibility. The optimization of the MLS cost function, a combination of ITSE, ITAE, MO, and MU, utilizes the population-based FLA [59][60] to determine the optimal controller parameters. FLA has been used in this work because of many properties, including its flexibility, ease of implementation, capacity to handle nonlinear optimization issues, and ability to steer clear of suboptimal areas. The proposed controller's performance is contrasted with the conventional PID for step, sine, and square reference trajectories. Simulations utilizing MATLAB R2023a are conducted to evaluate the efficacy of the proposed controller.

This paper's primary contributions involve:

- The gains of the WNN-based controller are optimized utilizing a state-of-the-art optimization algorithm known as FLA.
- A multi-objective cost function, incorporating performance indices such as ITSE, ITAE, MO, and MU, is employed to achieve an optimal transient response and minimize steady-state error.
- Parametric uncertainties and external disturbances are incorporated into the system model to rigorously assess and validate the effectiveness of the proposed WNN-based controller.

This paper's remaining sections are organized as follows: The magnetic levitation system's modeling is shown in Section II. The design and analysis of the suggested controller are presented in Sections III and IV. Optimization of the WNN parameters is presented in Section V. A detailed discussion and demonstration of the simulation's outcomes are provided in Section VI. The paper's conclusions are presented in Section VII, which also identifies areas for further research.

II. MAGNETIC LEVITATION SYSTEM MODEL

The MLS model utilized in this study is derived from the work presented in [61]. Fig. 1 presents a schematic representation of an MLS. The system employs an electromagnet to adjust the position of a magnetic ball through precise control of the current, which is governed by feedback derived from the ball's position. An optical sensor is integrated into the system to ensure accurate detection of the ball's position. The dynamic behavior of the ball is described by its equation of motion, which is expressed as follows:

$$m\frac{d^2y}{dt^2} = -k\frac{dy}{dt} + mg + F(y,i) \tag{1}$$

in which $F(y,i)$ represents the electromagnetic force produced by the electromagnet, with i denoting the electric current flowing through it. $y \geq 0$ denotes the vertical (downward) displacement of the ball, measured from a reference point, where $y = 0$ corresponds to the position of the ball adjacent to the coil. g represents the acceleration due to gravity, and k corresponds to the coefficient of viscous friction. The inductance of the electromagnet is influenced by the ball's position and can be mathematically modeled as follows:

$$L(y) = L_1 + \frac{L_0}{1+y/a} \tag{2}$$

where L_1, L_0, and a are defined as positive constants. Given $E(y,i) = \frac{1}{2}L(y)i^2$, which represents the energy stored in the electromagnet, the force $F(y,i)$ can be expressed as:

$$F(y,i) = \frac{\partial E}{\partial y} = -\frac{L_0 i^2}{2a(1+y/a)^2} \tag{3}$$

When the coil's electric circuit is powered by a voltage source with voltage v, Kirchhoff's voltage law establishes the relationship $v = \dot{\phi} + Ri$, where R represents the series resistance of the circuit, and $\phi = L(y)i$ corresponds to the magnetic flux linkage. By defining the state variables $x_1 = y, x_2 = \frac{dy}{dt}$ and $x_3 = i$, and considering the control input $u = v$, the state-space representation of the MLS can be derived as follows:

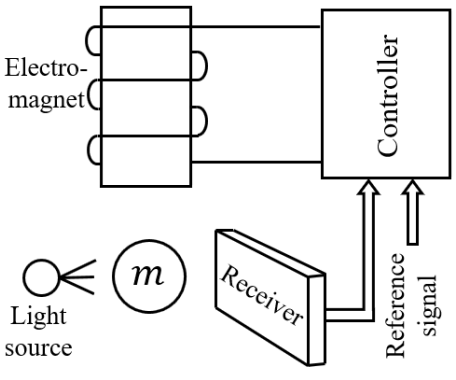

Fig. 1. Schematic diagram of a magnetic levitation system

$$\begin{aligned} \dot{x}_1 &= x_2 \\ \dot{x}_2 &= g - \frac{k}{m}x_2 - \frac{L_0 a x_3^2}{2m(a+x_1)^2} \\ \dot{x}_3 &= \frac{1}{L(x_1)}\left[-Rx_3 + \frac{L_0 a x_2 x_3}{(a+x_1)^2} + u\right] \end{aligned} \tag{4}$$

Table I provides a list of the nominal values for the parameters of the MLS.

TABLE I. MLS PARAMETERS

Parameter	Value
k	$0.001\ N/m/sec$
m	$0.1\ kg$
g	$9.81\ m/sec^2$
L_0	$0.01\ H$
L_1	$0.02\ H$
a	$0.05\ m$
R	$1\ \Omega$
$[u_{min}, u_{max}]$	$[0, 15]$

III. CONTROLLER DESIGN

The control strategy utilized in this paper leverages the wavelet neural network architecture, owing to its synergistic integration of wavelet theory and artificial neural network principles. The WNN effectively integrates the localization properties of wavelet transforms with the learning and generalization capabilities of artificial neural networks. This integration results in enhanced efficiency in identification and control tasks due to the WNN's inherent local specialization. Furthermore, the WNN exhibits a superior rate of parameter convergence compared to ANNs, achieving convergence within a reduced number of iterations.

The architecture of the WNN is presented in Fig. 2, which presents a Multiple-Input, Single-output (MISO) configuration. This architecture aligns favorably with a PID-like control structure for the MLS.

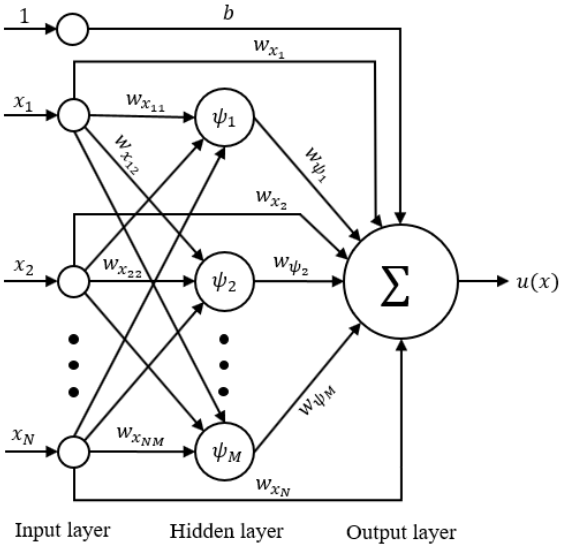

Fig. 2. Schematic representation of a MISO WNN architecture

Fig. 2 illustrates the three-layered structure of the WNN, comprising an input layer, a hidden layer, and an output layer. The number of input nodes N is dictated by the specific application. In the context of a PID-like controller, the input layer comprises four nodes: one for the error signal, one for its integral, one for its derivative, and one for the bias. The function of this layer is to transmit these input signals to the subsequent layers.

The hidden layer, also referred to as the mother wavelet layer, comprises multiple nodes, which are commonly referred to as wavelons. These nodes employ a family of wavelet functions as activation functions, which are derived from a mother wavelet by translation and dilation. The Mexican hat wavelet function is selected as the mother wavelet due to its smoothness, simplicity, zero-mean property, and computational efficiency. Its mathematical definition is as follows:

$$\psi(x) = (1 - x^2)exp\ (-0.5x^2) \tag{5}$$

The wavelet function associated with each node $\psi(z_j)$ is derived from the mother wavelet function through the following transformation:

$$\psi(z_j) = (1 - {z_j}^2)exp\ (-0.5{z_j}^2) \tag{6}$$

with $z_j = d_j \left(\sum_{i=1}^{N} w_{x_{ij}} x_i\right) - t_j$. This definition of z_j is referred to as a modified ridge network. In this formulation, t_j and d_j represent the translation and dilation factors of the wavelets, respectively. The number of nodes in the hidden layer M is contingent upon the complexity of the nonlinearity inherent in the application. Various methodologies exist for determining the optimal number of nodes in this layer. The methodology employed in this study to determine the optimal number of nodes in the hidden layer involves an iterative process. Initially, a single node is utilized, and the tracking error performance of the system is evaluated. Subsequently, the number of nodes is incrementally increased until satisfactory tracking error performance is attained. It is noteworthy that optimal tracking error performance was achieved with a single hidden node. Increasing the number of hidden nodes did not yield further improvements in tracking error performance but rather introduced additional complexity.

The output layer, comprising a single node, generates a linear combination of the weighted outputs from both the hidden and input nodes. This output, representing the control signal, can be expressed as follows:

$$u(x) = \sum_{j=1}^{M} w_{\psi_j} \psi(z_j) + \sum_{i=1}^{N} w_{x_i} x_i + b \tag{7}$$

Fig. 3 presents a comprehensive depiction of the closed-loop control system for the MLS, incorporating the proposed WNN-based controller.

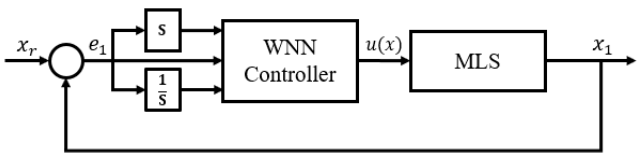

Fig. 3. Block diagram of WNN-Based MLS control

IV. STABILITY ANALYSIS

The augmented dynamic model of the MLS, incorporating both matched external disturbances d and parametric uncertainties, is represented by the following equation (8).

$$\begin{aligned}\dot{x} &= f(x,u)\\ \dot{x}_1 &= x_2\\ \dot{x}_2 &= g - \frac{k}{m}x_2 - \frac{L_0 a x_3^2}{2m(a+x_1)^2}\\ \dot{x}_3 &= \frac{1}{L(x_1)}\left[-Rx_3 + \frac{L_0 a x_2 x_3}{(a+x_1)^2} + u + d\right]\\ \dot{x}_4 &= e_1\end{aligned} \tag{8}$$

an augmented state, denoted as x_4, is introduced to emulate the integral action of the PID-like WNN-based controller. The parameters k, m, a, L_0, L_1, and R are represented as the sum of their nominal values and corresponding perturbations. For instance, the mass m is expressed as $m = m_0 + \delta_m$, where m_0 represents the nominal mass and δ_m denotes the perturbation. The error signal e_1 is calculated as the deviation of the system's current state x_1 from the reference trajectory x_r, expressed as $e_1 = x_1 - x_r$.

The control signal, utilizing the proposed controller with a single hidden node, is formulated as:

$$u = w_{\psi_1}\psi(z_1) + w_{e_1}e_1 + w_{e_2}e_2 + w_{\bar{e}_3}\bar{e}_3 + b \tag{9}$$

where $e_2 = x_2 - \dot{x}_r$, $\bar{e}_3 = x_4$ and $z_1 = d_1\left(w_{e_{11}}e_1 + w_{e_{21}}e_2 + w_{\bar{e}_{31}}\bar{e}_3\right) - t_1$. To determine the steady-state values of the system states, denoted as x_{ss}, the state derivatives $\dot{x}$ are set to zero. This operation yields a system of algebraic equations that can be subsequently solved to obtain the steady-state solution. Under steady-state conditions, with a step-like reference signal applied $x_1 = x_r$ and assuming the absence of external disturbances $d = 0$ and the utilization of nominal values for uncertain parameters, the system achieves the following steady-state conditions:

$$\begin{aligned}x_{1ss} &= x_r\\ x_{2ss} &= 0\\ x_{3ss} &= \left(2m_0 g(a_0 + x_r)^2 / L_{0_0} a_0\right)^{1/2}\\ Rx_{3ss} &= w_{\psi_1}\psi_1\left(d_1\left(w_{\bar{e}_3}x_{4ss}\right) - t_1\right) + +w_{\bar{e}_3}x_{4ss} + b\end{aligned} \tag{10}$$

for the specific numerical values provided in Tables I and III and under the proposed controller, where $x_r = 0.05$, the steady-state values are determined as follows: $x_{ss} = [0.05, 0, 6.264, \ -0.00485]^T$.

To analyze the stability characteristics of the system under the proposed controller, the system (4) is linearized around the steady-state operating point x_{ss} assuming the absence of external disturbances $d = 0$ and utilizing the nominal values of the uncertain parameters. The resulting linearized system dynamics can be expressed as:

$$\dot{e} = Ae \tag{11}$$

where

$$A = \frac{\partial f}{\partial x}\Big|_{x=x_{ss}} = \begin{bmatrix} 0 & 1 & 0 & 0 \\ 196.1884 & -0.01 & -3.1320 & 0 \\ 3.79 \cdot 10^5 & 3.00 \cdot 10^4 & -40 & 8.18 \cdot 10^5 \\ 1 & 0 & 0 & 0 \end{bmatrix},$$

and $e = x - x_{ss}$. The eigenvalues of A are listed in Table II.

TABLE II. MLS PARAMETERS

Eigenvalue	Value
$eig1$	$-13.6979 + 305.4084i$
$eig2$	$-13.6979 - 305.4084i$
$eig3$	-9.8216
$eig4$	-2.7925

Given that all eigenvalues of the matrix A possess negative real parts, it can be concluded that the linearized system exhibits exponential stability under the proposed controller. This implies that the error signal e converges to zero exponentially as time approaches infinity, $\lim_{t\to\infty} e = 0$, signifying that the state variable x_1 tracks the reference signal x_r exponentially.

V. WNN PARAMETERS OPTIMIZATION

As evident from Section III, the number of parameters requiring optimization is substantial. Furthermore, this number increases rapidly with an increase in the number of nodes in the input and hidden layers. Therefore, it is essential to employ an optimization method that guarantees the convergence of the parameters. When it comes to optimizing the parameters of a WNN, there are broadly two categories of methods: gradient-based and gradient-free. Gradient-based methods are susceptible to becoming trapped in local minima, which hinders the WNN parameters from converging to the optimal solution. Gradient-free methods, including evolutionary algorithms, offer an alternative that does not require gradient calculations. The parameters in Equation (7) are adjusted through the optimization process to minimize the cost function. Parameters are initialized randomly, and the lower and upper bounds for the parameters are determined based on empirical observations or through a process of trial and error.

A. Cost Function

The solution generated by the optimization algorithm is evaluated using a cost function. The cost function is typically a function of performance metrics that are to be optimized. For minimization problems, lower cost function values correspond to more optimal solutions. Numerous cost functions are employed in control system optimization. Some commonly used cost functions quantify tracking error, such as the Integral of Squared Error (ISE), Integral of Absolute Error (IAE), ITSE, ITAE, and Mean Squared Error (MSE). Other cost functions incorporate measures of transient response characteristics, such as overshoot and undershoot. Each of these cost functions influences specific characteristics of the transient response and steady-state error. The selected cost function is described below:

$$J_{FLA}(w) = ITSE + ITAE + 10 \cdot MO + 3 \cdot MU \tag{12}$$

where the w is the vector of parameters to be optimized, $ITSE = \int_0^T te^2(t)dt$, and $ITAE = \int_0^T t|e(t)|dt$. This cost function (12) is selected to combine the advantages of individual metrics, resulting in an improved transient response with minimal steady-state error. Specifically, it was designed to penalize overshoot and undershoot, reduce transient and steady-state errors, achieve faster settling times,

and minimize oscillations, particularly when training the MLS to track a challenging square wave reference.

B. Fick's Law Algorithm

The FLA is a metaheuristic optimization algorithm that leverages Fick's law of diffusion. This law describes the inherent tendency of particles, undergoing random thermal motion, to migrate from regions of high concentration to regions of low concentration. The FLA operates through three distinct stages: the diffusion phase, the equilibrium phase, and the steady-state phase. The FLA is regarded as an efficient and robust optimization algorithm due to its capability to achieve a well-balanced interaction among these three phases.

The primary stages of the FLA algorithm encompass the following key steps.

1. Initialization of the optimization parameters.
2. Clustering the population into two equal groups.
3. Transfer function.
4. Updating molecule position.

For a detailed explanation of the FLA, please refer to [59].

VI. Simulation Results and Analysis

In this section, the simulation model of the proposed WNN-based controller is constructed using MATLAB R2023a Simulink to evaluate and confirm its efficacy. The ball's initial position is set to $0\ m$ (neutral position), and the MLS has an operational range of $0.1\ m$. To ensure high precision and accuracy in the simulation results, a sampling time of 1 millisecond is employed. The performance of the proposed WNN-based controller is carefully assessed by contrasting it with a conventional PID controller, which assists as a benchmark for assessment. Three distinct reference trajectories (step, sinusoidal, and square waves) are utilized in the comparative simulations to provide a comprehensive assessment. To test the controller's rigidity under varying conditions and to represent a wide range of dynamic behaviors, these trajectories are chosen. Furthermore, to validate the flexibility and robustness of the proposed WNN-based controller, simulations are run while purposely exposing the MLS model to parameter uncertainties with 60% in m and 20% in k, R, a, L_0, L_1 in addition to large external disturbances, $d = 1 \cdot \sin(t)$. Under challenging and realistic working scenarios, this method guarantees that the controller's performance is established. To ensure a fair comparison, the gains of both controllers were optimized using the FLA with the same cost function. The optimization process was conducted under nominal conditions for the MLS parameters, with no external disturbances present. A square wave was employed as the reference signal due to its challenging nature for tracking, making it a rigorous test for the controllers. Table III presents the FLA parameter values used for both the WNN-based and PID controllers.

Table IV presents the optimized gains for both the WNN-based controller and the PID controller.

TABLE III. Values of Key Parameters for FLA

Parameter	Value	
	WNN-controller	**PID controller**
Number of Optimization Variables	10	3
Population Size	50	50
Maximum Iterations	2	2
Number of runs	1	1

TABLE IV. Optimized Gains for WNN-Based and PID Controllers, Including Lower and Upper Bounds Used in the FLA Optimization.

Optimal gain	Value	Lower and upper bounds
w_{ψ_1}	19.7619	[0 100]
$w_{e_{11}}$	50.5947	[0 100]
$w_{e_{21}}$	41.0184	[0 100]
$w_{e_{31}}$	33.2628	[0 100]
d_1	−4.5374	[−50 50]
t_1	27.5739	[−50 50]
w_{e_1}	9490.1114	[0 10000]
w_{e_2}	750.2516	[0 10000]
w_{e_3}	20461.3188	[0 100000]
b	100	[0 100]
k_p	8886.1994	[0 10000]
k_i	7041.6060	[0 10000]
k_d	561.3999	[0 10000]

A. Square Signal

By utilizing square wave as a reference signal, the tracking performance of the conventional PID controller and proposed WNN-based controller for the MLS is assessed. The reference signal was applied for 25 seconds. The square wave equation is expressed as:

$$x_r = 0.05 + 0.01 sign(sin(0.5t)) \quad (13)$$

The low-frequency excitation signal is used because the system's dynamics ensure that the assessment is consistent with the MLS's working characteristics.

Under, nominal conditions, the existence of parameter uncertainties, and external disturbances, Fig. 4 demonstrate the tracking performance of the WNN-based and PID controllers. With its carefully selected parameters, the WNN-based controller achieves accurate tracking of the reference trajectory with a small overshoot, very small steady-state error, and settling time of 1.39 seconds as shown in Fig. 4 (left). On the other hand, as shown in Fig. 4 (right), significantly longer settling times and larger overshoots are observed when utilizing the PID controller due to unacceptable handling of the parameter uncertainties and external disturbances.

Fig. 5 illustrates a comparison of the controller action of the WNN-based and PID controllers. The proposed WNN-based controller delivers a lower value of control action than the PID controller. This demonstrates that the WNN-based controller is more efficient in terms of energy consumption. This energy efficiency is kept both without and with parameter uncertainties and external disturbances, stressing the WNN-based controller's superior performance and robustness. The results highlight the WNN-based controller's ability to bring dependable and efficient control, even under challenging conditions.

The numerical values for overshoot, undershoot, and settling time pertaining to the WNN-based and PID controllers are detailed in Table V. Furthermore, the table includes the integral of squared error (ISE) and the integral of squared control input (ISU). The data presented in this table unequivocally demonstrates the energy efficiency of the WNN-based controller.

B. Sine Signal

A sine wave is used as the reference trajectory for the ball position of the MLS to assess the tracking performance of the control system. Explicitly, this reference signal is defined as:

$$x_r = 0.05 + 0.01(sin(0.5t)) \quad (14)$$

To test the tracking abilities of the system, the reference signal is applied for 25 seconds, to guarantee a smooth and reliable trajectory. This arrangement permits an inclusive valuation of the controller's capability to track periodic and dynamic reference motions, which is demonstrative of real-world operational situations. A valuable intuition into the performance of the system under sinusoidal reference inputs is provided by the results, stressing its ability to sustain accurate tracking.

Comparative tracking performance of the PID controller against the proposed WNN-based controller under nominal, parameter uncertainties, and external disturbances are illustrated in Fig. 6. This figure highlights the robustness and superiority of the proposed WNN-based controller in handling parametric uncertainties and external disturbances. Specifically, parameter uncertainties and external disturbances have a significant impact on the sinusoidal response of the PID controller, resulting in unacceptable tracking performance. However, the proposed WNN-based controller successfully maintains accurate tracking without degradation in performance while managing these uncertainties.

Furthermore, Fig. 7 illustrates that the proposed WNN-based controller provides a lower value for control action compared to the PID controller. In other words, the proposed WNN-based controller is more effective in terms of energy consumption than the PID controller, both in the absence and presence of parameter uncertainties and external disturbances. These Benefits make the WNN-based controller a very efficient and consistent control approach for the MLS, particularly in uncertain and dynamic operational environments.

The superiority of the proposed controller, regarding overshoot, settling time, and energy efficiency, is clearly supported by the numerical performance indices in Table V.

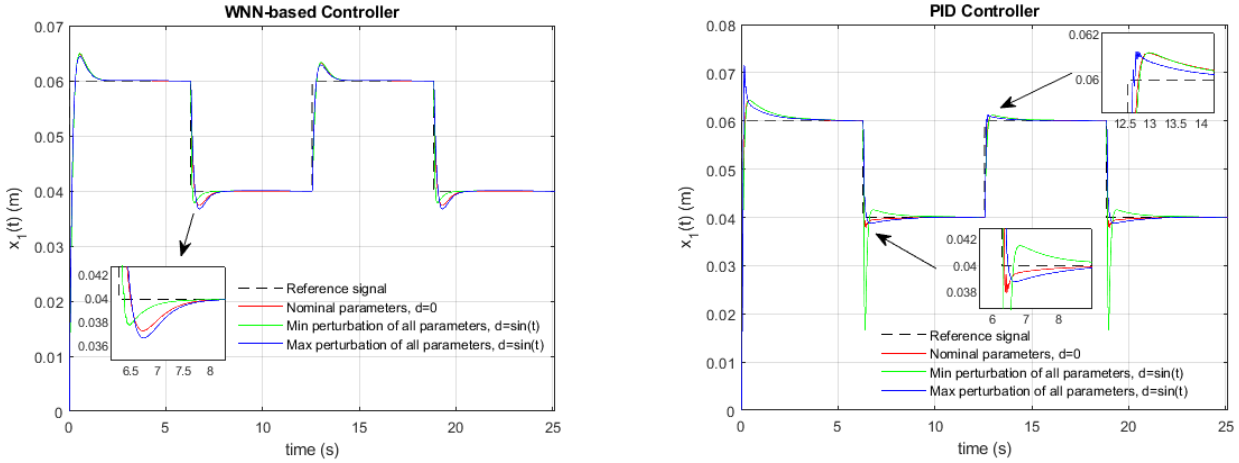

Fig. 4. MLS response to a square wave reference signal with WNN-based and PID controllers, showing the effects of parameter perturbations and external disturbance

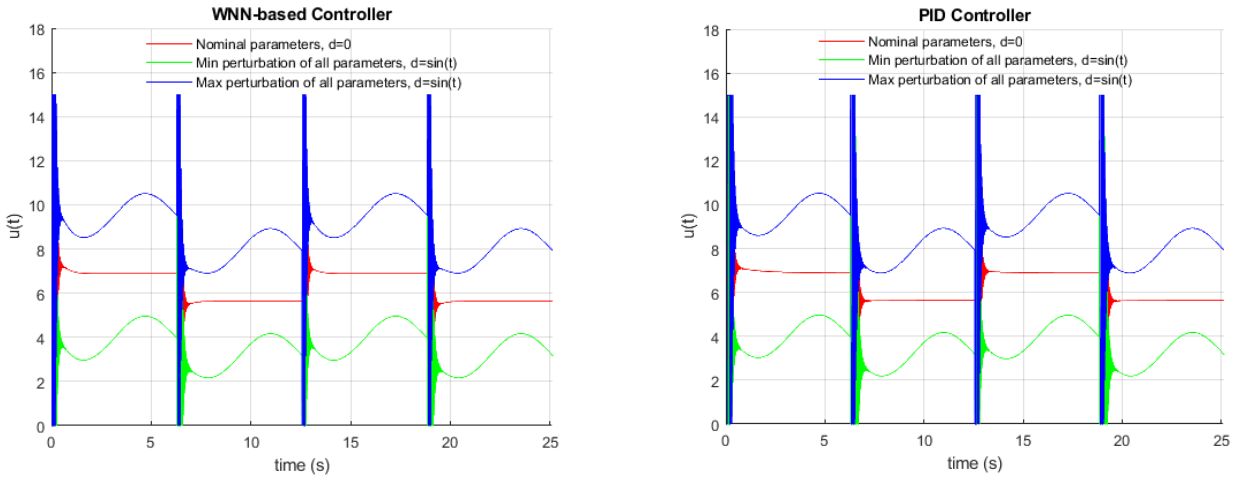

Fig. 5. Control action of WNN-based and PID controllers for square wave tracking, showing saturation limits between 0 and 15

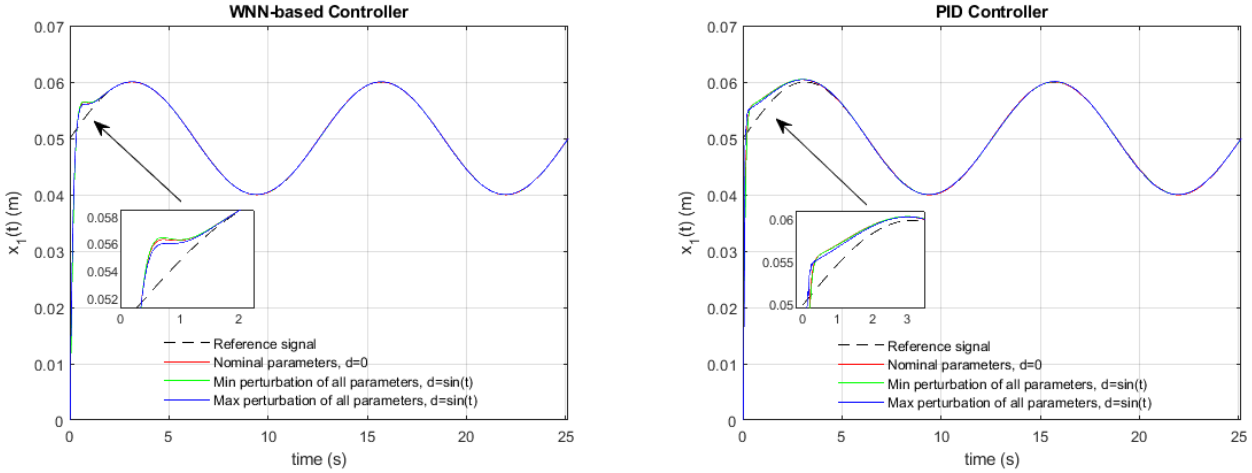

Fig. 6. MLS response to a square sine reference signal with WNN-based and PID controllers, showing the effects of parameter perturbations and external disturbance

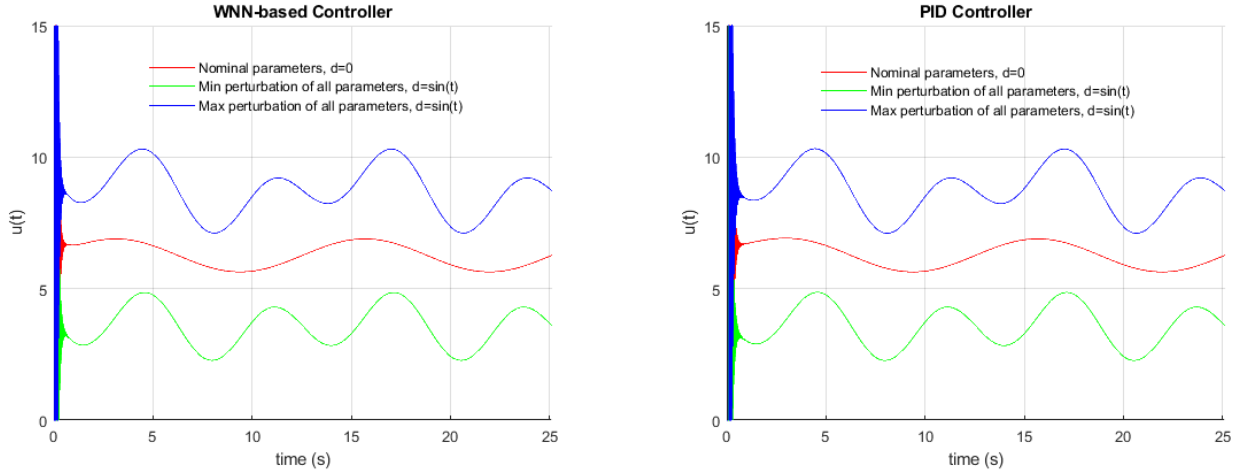

Fig. 7. Control action of WNN-based and PID controllers for sine wave tracking, showing saturation limits between 0 and 15

TABLE V. EVALUATION OF OPTIMIZED WNN-BASED AND PID CONTROLLER PERFORMANCE UNDER VARIOUS CONDITIONS.

Controller	Reference signal	Parameter and external disturbance variations	Settling time (sec.)	Min undershoot or Max overshoot %	ISE	ISU
WNN-based	Square	Nominal parameters, d=0	1.39	8.00	0.0003769	1031.58
		Min. perturbation of all parameters, d=sin(t)	1.39	8.28	0.0003726	360.59
		Max. perturbation of all parameters., d=sin(t)	1.39	7.33	0.0003700	1973.50
PID	Square	Nominal parameters, d=0	5.43	7.25	0.0002870	1044.99
		Min. perturbation of all parameters, d=sin(t)	5.43	58.22	0.0003898	367.93
		Max. perturbation of all parameters., d=sin(t)	5.43	19.17	0.0002941	1992.51
WNN-based	Sine	Nominal parameters, d=0	2.00	5.47	0.0001587	1000.82
		Min. perturbation of all parameters, d=sin(t)	2.00	5.71	0.0002221	338.94
		Max. perturbation of all parameters., d=sin(t)	2.00	4.79	0.0001969	1938.44
PID	Sine	Nominal parameters, d=0	5.00	6.86	0.0001552	1005.88
		Min. perturbation of all parameters, d=sin(t)	5.00	6.73	0.0001631	342.05
		Max. perturbation of all parameters., d=sin(t)	5.00	6.35	0.0001468	1948.83
WNN-based	Step	Nominal parameters, d=0	2.00	6.38	0.0002098	994.09
		Min. perturbation of all parameters, d=sin(t)	2.00	6.70	0.0002212	336.91
		Max. perturbation of all parameters., d=sin(t)	2.00	5.70	0.0001960	1930.47
PID	Step	Nominal parameters, d=0	6.00	7.16	0.0001538	1000.72
		Min. perturbation of all parameters, d=sin(t)	6.00	7.08	0.0001617	339.95
		Max. perturbation of all parameters., d=sin(t)	6.00	7.04	0.0001453	1940.68

C. Step Signal

The MLS model is exposed to an input scenario where it accepts the reference step input. Explicitly, the reference step inputs are defined as:

$$x_r = 0.05 \quad (15)$$

To assess the capability of the system to track the desired ball position, the step input is applied simultaneously over a simulation period of 10 seconds. The results of this simulation deliver a valuable vision of the behavior of the system and its ability to attain accurate control of the ball position under such circumstances.

The tracking performance of the conventional PID controller is compared with that of the proposed WNN-based controller as shown in Fig. 8. The comparison is run without and with MLS parameter uncertainties and external disturbances. It can be noticed from Fig. 8 that while both the PID and proposed WNN-based controllers reveal some ability to handle external disturbances and parametric uncertainties, they struggle to control the overshoot, which exceeds 10% in all cases. However, the settling time for the PID controller is more than twice that of the proposed WNN-based controller.

Furthermore, Fig. 9 illustrates the control action for both the PID and proposed WNN-based controllers. The proposed WNN-based controller delivers a lesser value of control action. This implies that the proposed controller is less energy consumption than the PID controller, particularly under situations of large external disturbances and parametric uncertainties.

Table V's numerical performance indices conclusively prove the efficacy of the proposed controller in terms of overshoot, settling time, and energy efficiency

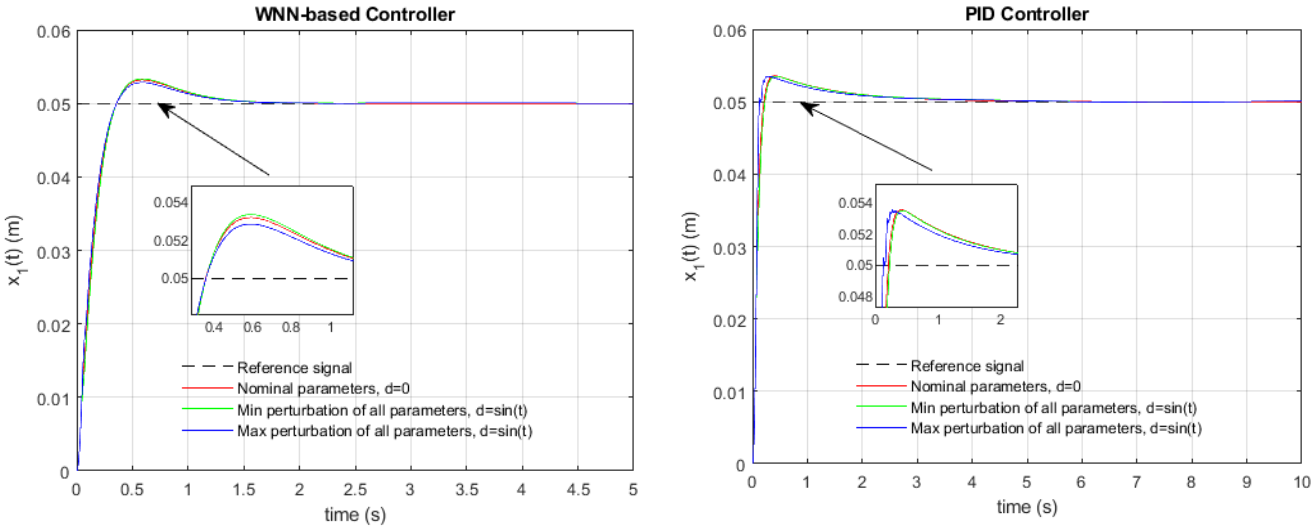

Fig. 8. MLS response to a step reference signal with WNN-based and PID controllers, showing the effects of parameter perturbations and external disturbance

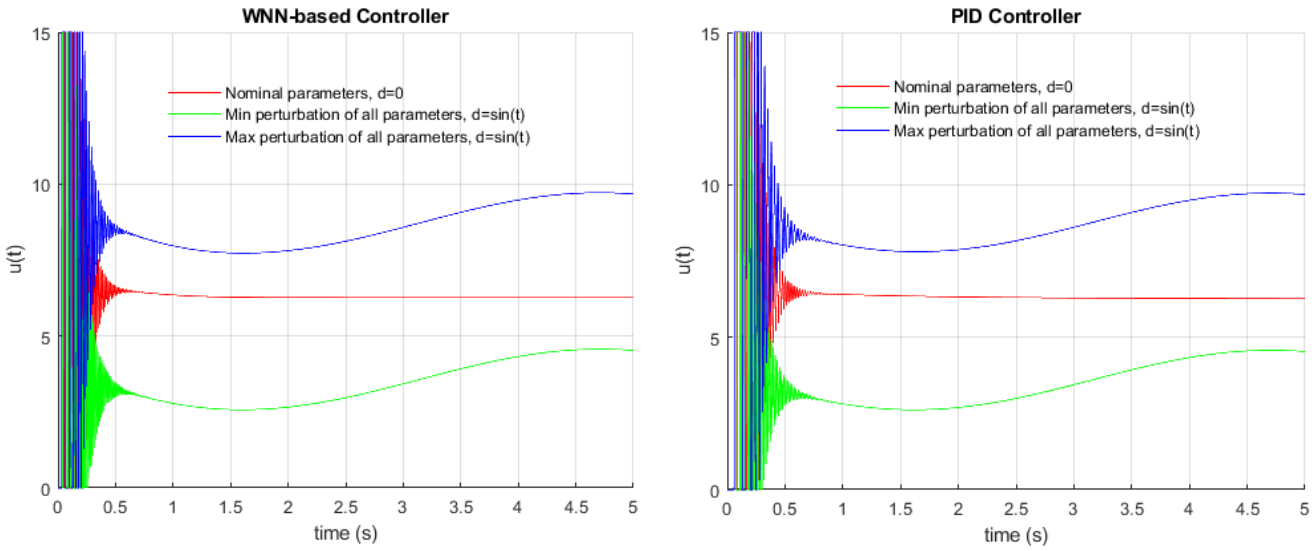

Fig. 9. Control action of WNN-based and PID controllers for step tracking, showing saturation limits between 0 and 15

VII. CONCLUSION

This work presented the design of a nonlinear controller based on a wavelet neural network. The controller gains were optimized using the FLA algorithm, resulting in enhanced transient response and minimal steady-state error. The proposed controller exhibited excellent transient response characteristics and demonstrated robustness in the face of external disturbances and parameter uncertainties. It effectively rejected a significant external disturbance, $d = 1 \cdot \sin(t)$, and maintained stability and excellent performance despite a 60% uncertainty in the ball mass and 20% uncertainty in other system parameters. To evaluate its performance, the proposed controller was compared to a conventional PID controller using a set of three reference trajectories: step, sinusoidal, and square waves. Simulation results demonstrated that the proposed controller exhibited superior transient response characteristics compared to the PID controller in terms of overshoot, steady-state error, and energy consumption, even under conditions of external disturbances and the parameter uncertainties described above. A promising future direction involves the experimental implementation and evaluation of the proposed controller on a real-world MLS.

REFERENCES

[1] M. Jastrzębski and J. Kabziński, "Adaptive control of magnetic levitation system based on fuzzy inversion," *Scientific Reports*, vol. 14, no. 1, Oct. 2024, doi: 10.1038/s41598-024-76067-9.

[2] Z. Deng, L. Wang, H. Li, J. Li, H. Wang, and J. Yu, "Dynamic Studies of the HTS Maglev Transit System," *IEEE Transactions on Applied Superconductivity*, vol. 31, no. 5, pp. 1–5, Aug. 2021, doi: 10.1109/tasc.2021.3052452.

[3] I. Iswanto and A. Ma'arif, "Robust Integral State Feedback Using Coefficient Diagram in Magnetic Levitation System," *IEEE Access*, vol. 8, pp. 57003–57011, 2020, doi: 10.1109/access.2020.2981840.

[4] S. R. Dabbagh, M. M. Alseed, M. Saadat, M. Sitti, and S. Tasoglu, "Biomedical Applications of Magnetic Levitation," *Advanced NanoBiomed Research*, vol. 2, no. 3, Dec. 2021, doi: 10.1002/anbr.202100103.

[5] J. Xie, P. Zhao, C. Zhang, J. Fu, and L.-S. Turng, "Current state of magnetic levitation and its applications in polymers: A review," *Sensors and Actuators B: Chemical*, vol. 333, p. 129533, Apr. 2021, doi: 10.1016/j.snb.2021.129533.

[6] L. Zhou and J. Wu, "Magnetic Levitation Technology for Precision Motion Systems: A Review and Future Perspectives," *International Journal of Automation Technology*, vol. 16, no. 4, pp. 386–402, Jul. 2022, doi: 10.20965/ijat.2022.p0386.

[7] S. Ge *et al*., "Magnetic Levitation in Chemistry, Materials Science, and Biochemistry," *Angewandte Chemie International Edition*, vol. 59, no. 41, pp. 17810–17855, Aug. 2020, doi: 10.1002/anie.201903391.

[8] P. Carneiro *et al*., "Electromagnetic energy harvesting using magnetic levitation architectures: A review," *Applied Energy*, vol. 260, p. 114191, Feb. 2020, doi: 10.1016/j.apenergy.2019.114191.

[9] B. Karakuzu *et al*., "Magnetic levitation-based miniaturized technologies for advanced diagnostics," *Emergent Materials*, Jul. 2024, doi: 10.1007/s42247-024-00762-6.

[10] T. Halawa, "Numerical and Experimental Investigation of the Performance of a Vertical Axis Wind Turbine Based on the Magnetic Levitation Concept," *Journal of Energy Resources Technology*, vol. 144, no. 9, Feb. 2022, doi: 10.1115/1.4053577.

[11] M. Fekry and S. Yoshida, "Aeroelastic numerical simulation of a magnetically levitated horizontal axis wind turbine," *Sustainable Energy Technologies and Assessments*, vol. 43, p. 100899, Feb. 2021, doi: 10.1016/j.seta.2020.100899.

[12] Y. Liu, K. Fan, and Q. Ouyang, "Intelligent Traction Control Method Based on Model Predictive Fuzzy PID Control and Online Optimization for Permanent Magnetic Maglev Trains," *IEEE Access*, vol. 9, pp. 29032–29046, 2021, doi: 10.1109/access.2021.3059443.

[13] Y. Xu, K. Fan, Q. Hu, and X. Zhang, "Positioning of Suspended Permanent Magnet Maglev Trains Using Satellite–Ground Multisensor Fusion," *IEEE Sensors Journal*, vol. 24, no. 10, pp. 16816–16825, May 2024, doi: 10.1109/jsen.2024.3384699.

[14] Y. Jiang, Y. Deng, P. Zhu, M. Yang, and F. Zhou, "Optimization on Size of Halbach Array Permanent Magnets for Magnetic Levitation System for Permanent Magnet Maglev Train," *IEEE Access*, vol. 9, pp. 44989–45000, 2021, doi: 10.1109/access.2021.3058124.

[15] M. M. Alseed, S. Rahmani Dabbagh, P. Zhao, O. Ozcan, and S. Tasoglu, "Portable magnetic levitation technologies," *Advanced Optical Technologies*, vol. 10, no. 2, pp. 109–121, Apr. 2021, doi: 10.1515/aot-2021-0010.

[16] D. K. Supreeth, S. I. Bekinal, S. R. Chandranna, and M. Doddamani, "A Review of Superconducting Magnetic Bearings and Their Application," *IEEE Transactions on Applied Superconductivity*, vol. 32, no. 3, pp. 1–15, Apr. 2022, doi: 10.1109/tasc.2022.3156813.

[17] S. Zheng and C. Wang, "Rotor Balancing for Magnetically Levitated TMPs Integrated With Vibration Self-Sensing of Magnetic Bearings," *IEEE/ASME Transactions on Mechatronics*, vol. 26, no. 6, pp. 3031–3039, Dec. 2021, doi: 10.1109/tmech.2021.3051372.

[18] R. Bonetti, D. Bortis, L. Beglinger, and J. W. Kolar, "Exploring the Physical Limits of Axial Magnetic Bearings Featuring Extremely Large Vertical Levitation Distances," *IEEE Transactions on Industry Applications*, vol. 57, no. 6, pp. 6931–6943, Nov. 2021, doi: 10.1109/tia.2021.3096170.

[19] S. Dey, S. Banerjee, and J. Dey, "Practical Application of Fractional-Order PID Controller based on Evolutionary Optimization Approach for a Magnetic Levitation System," *IETE Journal of Research*, vol. 69, no. 11, pp. 8168–8192, Mar. 2022, doi: 10.1080/03772063.2022.2052983.

[20] C. Lyu, C. Zhang, D. Tang, and P. Zhao, "Magnetic Levitation in Medicine and Bioengineering," *Magnetic Levitation*, pp. 163–179, 2024, doi: 10.1007/978-981-99-8314-8_9.

[21] Q. Chen, Y. Tan, J. Li, and I. Mareels, "Decentralized PID Control Design for Magnetic Levitation Systems Using Extremum Seeking," *IEEE Access*, vol. 6, pp. 3059–3067, 2018, doi: 10.1109/access.2017.2787052.

[22] A. Ghosh, T. Rakesh Krishnan, P. Tejaswy, A. Mandal, J. K. Pradhan, and S. Ranasingh, "Design and implementation of a 2-DOF PID compensation for magnetic levitation systems," *ISA Transactions*, vol. 53, no. 4, pp. 1216–1222, Jul. 2014, doi: 10.1016/j.isatra.2014.05.015.

[23] A. Mughees and S. A. Mohsin, "Design and Control of Magnetic Levitation System by Optimizing Fractional Order PID Controller Using Ant Colony Optimization Algorithm," *IEEE Access*, vol. 8, pp. 116704–116723, 2020, doi: 10.1109/access.2020.3004025.

[24] M. Qasim, A. I. Abdulla, and A. B. Ayoub, " Design of a Robust Component-wise Sliding Mode Controller for a Two-Link Manipulator," *Journal of Robotics and Control (JRC)*, vol. 6, no. 2, pp. 527–534, doi: 10.18196/jrc.v6i2.25632.

[25] B. Oppeneiger *et al*., "Model predictive control of a magnetic levitation system with prescribed output tracking performance," *Control Engineering Practice*, vol. 151, p. 106018, Oct. 2024, doi: 10.1016/j.conengprac.2024.106018.

[26] M. Qasim, A. B. Ayoub, and A. I. Abdulla, "NMPC Based-Trajectory Tracking and Obstacle Avoidance for Mobile Robots," *International Journal of Robotics and Control Systems*, vol. 4, no. 4, pp. 2026–2040, Nov. 2024, doi: 10.31763/ijrcs.v4i4.1605.

[27] W. Hu, Y. Zhou, Z. Zhang, and H. Fujita, "Model Predictive Control for Hybrid Levitation Systems of Maglev Trains With State Constraints," *IEEE Transactions on Vehicular Technology*, vol. 70, no. 10, pp. 9972–9985, Oct. 2021, doi: 10.1109/tvt.2021.3110133.

[28] W. Hu, Y. Zhou, Z. Zhang, and H. Fujita, "Model Predictive Control for Hybrid Levitation Systems of Maglev Trains With State Constraints," *IEEE Transactions on Vehicular Technology*, vol. 70, no. 10, pp. 9972–9985, Oct. 2021, doi: 10.1109/tvt.2021.3110133.

[29] O. Y. Ismael, M. Almaged, and A. I. Abdulla, "Nonlinear Model Predictive Control-based Collision Avoidance for Mobile Robot," *Journal of Robotics and Control (JRC)*, vol. 5, no. 1, pp. 142–151, Jan. 2024, doi: 10.18196/jrc.v5i1.20615

[30] M. N. Alghanim, M. Qasim, K. P. Valavanis, M. J. Rutherford, and M. Stefanovic, "Comparison of Controller Performance for UGV-Landing Platform Self-Leveling," *2020 28th Mediterranean Conference on Control and Automation (MED)*, Sep. 2020, doi: 10.1109/med48518.2020.9182837.

[31] M. N. Alghanim, M. Qasim, K. P. Valavanis, M. J. Rutherford, and M. Stefanovic, "Passivity-Based Adaptive Controller for Dynamic Self-Leveling of a Custom-Built Landing Platform on Top of a UGV," *2020 28th Mediterranean Conference on Control and Automation (MED)*, Sep. 2020, doi: 10.1109/med48518.2020.9182807.

[32] M. Qasim and O. Y. Ismael, "Shared Control of a Robot Arm Using BCI and Computer Vision," *Journal Européen des Systèmes Automatisés*, vol. 55, no. 1, pp. 139–146, Feb. 2022, doi: 10.18280/jesa.550115.

[33] M. N. Noaman, M. Qasim, and O. Y. Ismael, "Landmarks exploration algorithm for mobile robot indoor localization using VISION sensor," *Journal of Engineering Science & Technology*, vol. 16, no. 4, pp. 3165-3184, 2021.

[34] J. Zhang, X. Wang, and X. Shao, "Design and Real-Time Implementation of Takagi–Sugeno Fuzzy Controller for Magnetic Levitation Ball System," *IEEE Access*, vol. 8, pp. 38221–38228, 2020, doi: 10.1109/access.2020.2971631.

[35] D. Zhang, Y. Sun, N. Jia, J. Xu, and W. Sun, "Adaptive Fuzzy Super-twisting Sliding Mode Control for the Multi-electromagnets Levitation System of Maglev Vehicles: Design and Experiments," *IEEE Transactions on Intelligent Vehicles*, pp. 1–11, 2024, doi: 10.1109/tiv.2024.3463632.

[36] M. Abdollahzadeh and M. Pourgholi, "Adaptive fuzzy sliding mode control of magnetic levitation system based on Interval Type-2 Fuzzy Neural Network Identification with an Extended Kalman–Bucy filter," *Engineering Applications of Artificial Intelligence*, vol. 130, p. 107645, Apr. 2024, doi: 10.1016/j.engappai.2023.107645.

[37] J. de J. Rubio *et al*., "Adapting H-infinity controller for the desired reference tracking of the sphere position in the maglev process," *Information Sciences*, vol. 569, pp. 669–686, Aug. 2021, doi: 10.1016/j.ins.2021.05.018.

[38] H. Chi, F. Meng, H. Chen, and Y. Zhang, "H-infinity Optimal Performance Design of Maglev Control System based on Bode Integral Constraint," *2022 IEEE 6th Advanced Information Technology, Electronic and Automation Control Conference (IAEAC)*, pp. 1423–1430, Oct. 2022, doi: 10.1109/iaeac54830.2022.9930067.

[39] J. Jose and S. J. Mija, "Design of H∞ Controller for Magnetic Levitation Systems," *2020 First IEEE International Conference on Measurement, Instrumentation, Control and Automation (ICMICA)*, pp. 1–6, Jun. 2020, doi: 10.1109/icmica48462.2020.9242769.

[40] O. Y. Ismael, M. Qasim, and M. N. Noaman, "Equilibrium Optimizer-Based Robust Sliding Mode Control of Magnetic Levitation System," *Journal Européen des Systèmes Automatisés*, vol. 54, no. 1, pp. 131–138, Feb. 2021, doi: 10.18280/jesa.540115.

[41] J. Wang, L. Zhao, and L. Yu, "Adaptive Terminal Sliding Mode Control for Magnetic Levitation Systems With Enhanced Disturbance Compensation," *IEEE Transactions on Industrial Electronics*, vol. 68, no. 1, pp. 756–766, Jan. 2021, doi: 10.1109/tie.2020.2975487.

[42] W. Wang, G. Yang, J. Yan, H. Ge, and P. Zhi, "Magnetic levitation planar motor and its adaptive contraction backstepping control for logistics system," *Advances in Mechanical Engineering*, vol. 13, no. 3, Mar. 2021, doi: 10.1177/16878140211004782.

[43] M. Wang, Z. Hao, Y. He, S. Zeng, Z. Qi, and P. Liu, "Active Disturbance Rejection Backstepping Cross-Coupling Controller Design for a Magnetic Levitation Vehicle Suspension Frame," *IEEE Transactions on Transportation Electrification*, pp. 1–1, 2024, doi: 10.1109/tte.2024.3467711.

[44] D. Wang, F. Meng, and S. Meng, "Linearization Method of Nonlinear Magnetic Levitation System," *Mathematical Problems in Engineering*, vol. 2020, pp. 1–5, Jun. 2020, doi: 10.1155/2020/9873651.

[45] B. Mansi, S. Nachiket, A. Sheikh, K. Sunny, and F. Kazi, "Parameter Estimator based Feedback Linearization Control strategy of Magnetic Levitation System," *2021 31st Australasian Universities Power Engineering Conference (AUPEC)*, pp. 1–6, Sep. 2021, doi: 10.1109/aupec52110.2021.9597715.

[46] O. Y. Ismael, M. Qasim, M. N. Noaman, and A. Kurniawan, "Salp Swarm Algorithm-Based Nonlinear Robust Control of Magnetic Levitation System Using Feedback Linearization Approach," *Proceedings of the 3rd International Conference on Electronics, Communications and Control Engineering*, Apr. 2020, doi: 10.1145/3396730.3396734.

[47] A. Fatemimoghadam, H. Toshani, and M. Manthouri, "Control of magnetic levitation system using recurrent neural network-based adaptive optimal backstepping strategy," *Transactions of the Institute of Measurement and Control*, vol. 42, no. 13, pp. 2382–2395, Apr. 2020, doi: 10.1177/0142331220911821.

[48] Y. Zheng and H.-J. Ahn, "Improvement of the Transient Levitation Response of a Magnetic Levitation System Using Hybrid Fuzzy and Artificial Neural Network Control," *International Journal of Precision Engineering and Manufacturing*, Nov. 2024, doi: 10.1007/s12541-024-01173-7.

[49] T. N. Truong, A. T. Vo, and H.-J. Kang, "Implementation of an Adaptive Neural Terminal Sliding Mode for Tracking Control of Magnetic Levitation Systems," *IEEE Access*, vol. 8, pp. 206931–206941, 2020, doi: 10.1109/access.2020.3036010.

[50] W. Yang, F. Meng, S. Meng, S. Man, and A. Pang, "Tracking Control of Magnetic Levitation System Using Model-Free RBF Neural Network Design," *IEEE Access*, vol. 8, pp. 204563–204572, 2020, doi: 10.1109/access.2020.3037352.

[51] T. Peng, H. Peng, and T. Kang, "RBF-ARX model-based trust region nonlinear model predictive control and its application on magnetic levitation ball system," *Nonlinear Dynamics*, vol. 113, no. 3, pp. 2521–2543, Sep. 2024, doi: 10.1007/s11071-024-10342-2.

[52] Y. Qin, H. Peng, F. Zhou, X. Zeng, and J. Wu, "Nonlinear modeling and control approach to magnetic levitation ball system using functional weight RBF network-based state-dependent ARX model," *Journal of the Franklin Institute*, vol. 352, no. 10, pp. 4309–4338, Oct. 2015, doi: 10.1016/j.jfranklin.2015.06.014.

[53] Y. Sun, J. Xu, H. Qiang, C. Chen, and G. Lin, "Adaptive sliding mode control of maglev system based on RBF neural network minimum parameter learning method," *Measurement*, vol. 141, pp. 217–226, Jul. 2019, doi: 10.1016/j.measurement.2019.03.006.

[54] B. Kumar, S. K. Swain, S. K. Mishra, Y. K. Singh, and S. Ghosh, "Radial Basis Function-based Adaptive Gain Super-Twisting Controller for Magnetic Levitation System with Time-Varying External Disturbance," *IEEE Transactions on Transportation Electrification*, vol. 10, no. 4, pp. 9121-9132, 2024, doi: 10.1109/tte.2024.3354795.

[55] Y. Sun, J. Xu, G. Lin, and N. Sun, "Adaptive neural network control for maglev vehicle systems with time-varying mass and external disturbance," *Neural Computing and Applications*, vol. 35, no. 17, pp. 12361–12372, Mar. 2021, doi: 10.1007/s00521-021-05874-2.

[56] Y. Xiao, X. Wang, Y. Zhao, and W. Liu, "Research on Dynamic Control Method of Loom Spindle Braking System Based on Fuzzy Neural Network," *IEEE Access*, vol. 10, pp. 116723–116734, 2022, doi: 10.1109/access.2022.3219211.

[57] Z. Ma, Z. Zhang, and X. Cai, "Robust adaptive control of voltage-type MLS based on wavelet neural network," *IFAC-PapersOnLine*, vol. 53, no. 2, pp. 9213–9218, 2020, doi: 10.1016/j.ifacol.2020.12.2194.

[58] S.-Y. Chen, Y.-C. Hung, Y.-H. Hung, and C.-H. Wu, "Application of a recurrent wavelet fuzzy-neural network in the positioning control of a magnetic-bearing mechanism," *Computers & Electrical Engineering*, vol. 54, pp. 147–158, Aug. 2016, doi: 10.1016/j.compeleceng.2015.11.022.

[59] F. A. Hashim, R. R. Mostafa, A. G. Hussien, S. Mirjalili, and K. M. Sallam, "Fick's Law Algorithm: A physical law-based algorithm for numerical optimization," *Knowledge-Based Systems*, vol. 260, p. 110146, Jan. 2023, doi: 10.1016/j.knosys.2022.110146.

[60] O. Y. Ismael, M. N. Noaman, and I. K. Abdullah, "Fick's Law Algorithm Based-Nonlinear Model Predictive Control of Twin Rotor MIMO System," *Journal of Robotics and Control (JRC)*, vol. 5, no. 3, pp. 694–705, 2024, doi: 10.18196/jrc.v5i3.21725.

[61] K. H. Khalil and J. W. Grizzle, *Nonlinear Systems*. Upper Saddle River, NJ, USA: Prentice Hall, 2002.